PRAJÑĀ - Journal of Pure and Applied Sciences Vol. 21: 38 - 43 (2013)
ISSN 0975 - 2595

A LINEAR SCALING LAW FOR ALKALINE-EARTH-METAL OXIDES: A THERMODYNAMIC ANALYSIS

N. K. Bhatt
Department of Physics, Sardar Patel University, Vallabh Vidyanagar 388 120, Gujarat, India

ABSTRACT

Density functional perturbation theory has been employed to compute phonon dynamics of alkaline-earth-metal oxides (MgO, CaO and SrO) in their cubic B1-phase. To solve Kohn-Sham density functional for core-electrons, ultrasoft pseudo-potentials with non-linear core correction within the generalized gradient approximation were used. High temperature thermodynamic properties were calculated within the harmonic approximation. These results are then used to scale vibrational free energy on the systematic behaviour of these oxides. We propose that based on the Born effective charge, zero-point energy and reduced mass of these compounds can be used to predict ionic radius of divalent barium ion (Ba^{+2}), zero-point energy, and finite temperature vibrational free energy and thus the entropy for its oxide, BaO. We show this simple scaling characterization procedure circumvents detailed calculations of lattice dynamics. We observe qualitative agreement for the computed thermal properties, and are discussed by treating these oxides within the proposed linear scaling criterion.

Keywords: *Alkaline-earth oxides, phonon dynamics, thermodynamics, DFT.*

INTRODUCTION

Although, the alkaline-earth-metal (A) binary oxides (O) (AO ≡ MgO, CaO, SrO, BaO) adopt a simple rocksalt crystal structure (also known as the B1-phase), interest remains in studying their thermophysical properties at high temperature and/or pressure. For instance, thermo-elastic evaluation of MgO and CaO is very important to explore properties of Earth's mantle [1] under simultaneous high pressure and temperature. Also, an increasing rise of performance-enhancing electronics (microelectronics) coupled with improve ICs performance constrained mostly due to the presence of high temperatures well beyond the limits of conventional Si-based electronics [2,3]. In this scenario, SrO and BaO are emerging as potential candidates for buffer layer in the epitaxial growth of multifunctional perovskite oxides on silicon; they replace SiO_2 in metal-oxide-semiconductor FET devices [3]. Thus, it is natural to examine the thermal response of these oxides at high-T condition on comparative merits for device engineering. In the present study, however, we exclude thermal characterization of BeO due to the following reason. It is known that for such ionic solids, the electron density of the valence electrons around the anions depends on the crystal structure. And since BeO crystallizes in hexagonal B8-phase, we cannot treat computed thermodynamic properties on an equal footing with other AOs due to different structural environment [4]. We also mention that Bonsquet et al. [5] have identified the thermal strain-induced ferroelectricity in the case of BaO; however, the present study is not intended to discuss such issues.

In the present paper, we therefore evaluate basic thermodynamic properties of MgO, CaO and SrO in B1-phase at finite temperatures using the harmonic approximation (HA) for phonon dynamics. Lattice dynamics is carried out using first principles density functional perturbation theory (DFPT) employing the generalized gradient approximation (GGA). Our interest is not only to evaluate thermophysical properties at high-T but also to draw general inferences for these oxides going from MgO → SrO in a systematic way. We also intend to examine whether the unified approach to these AOs can be adopted to compute vibrational response, and in turn the thermal properties without going in to details of actual calculations of phonon dynamics. We show that such unified approach leads to the vibrational free energy and entropy of BaO at finite temperatures, in general agreement with the recent *ab initio* calculations.

Computation

Alkaline-earth oxides (AOs) being ionic solids, the electronic excitation is diminutive up to moderately high temperatures (T ≤ Tm, the melting temperature). Thus, the entire solid-state thermal properties can be deduced from the lattice dynamics. In order to obtain equilibrium ground properties, and the phonon dispersion curve (pdc) and phonon density of state (p-dos), we have employed *ab initio* pseudopotential density functional theory [6]. To solve Kohn-Sham density functional for core-electrons, Vanderbilt ultrasoft pseudopotentials with non-linear core correction within the GGA [7] were used. We performed scalar relativistic calculations. A plane-wave basis set with a kinetic energy cut-off of 180, 250 and 250 Ry was used for MgO, CaO and SrO, respectively. Convergence test of 8x8x8 Monkhorst-Pack k-point grid for electronic Brillouin zone (BZ) integration deduce total energy to converge by 0.1 mRy. The ground state structural parameters are determined by calculating the self-consistent total energy in B1-phase. Atomic positions for cation (A^{+2}) and anion (O^{-2}) are taken as (0, 0, 0) and (½, ½, ½), respectively. Once the total energy for different cell volumes is obtained, it is fitted to the Murnaghan's equation of state [8] to obtain equilibrium lattice parameter a_o, bulk modulus B_0 and its first order pressure derivative B_0'.

The phonon spectra, the p-dos, and the effective charge were calculated by using DFPT as implemented in the Quantum Espresso code [6]. First, the dynamical matrix elements were calculated on a 4x4x4 k-grid and the real-space interatomic force constants were obtained by

*Corresponding author: *llll*

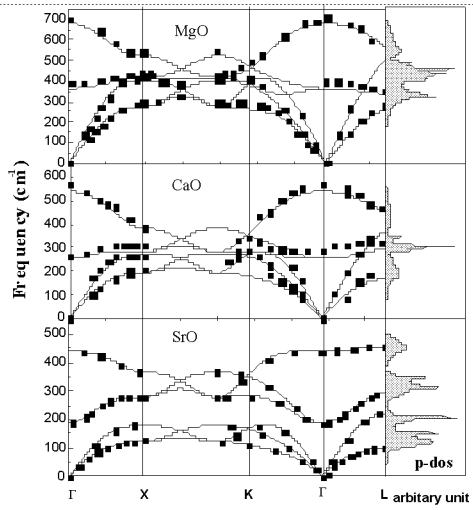

Fig: 1. Phonon dispersion curve and phonon density of states at T = 0 K. Experimental data are from Ref. [23-25]

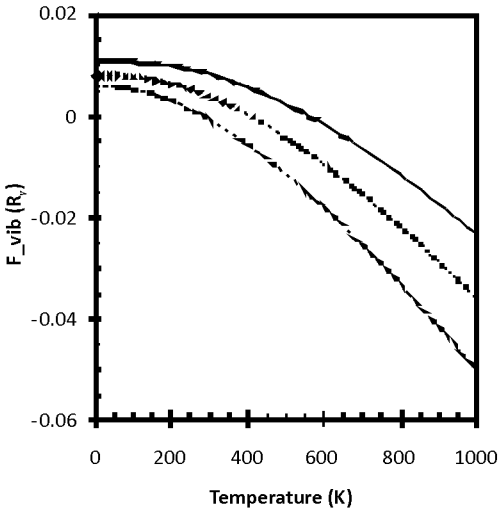

Fig: 2. Lattice vibrational free energy for MgO (continuous line), CaO (dotted line) and SrO (dashed line)

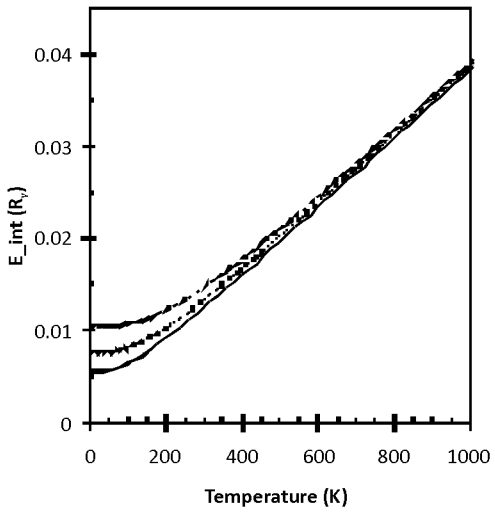

Fig: 3. Internal energy for three AO. Lines have the same meaning as the Fig: 2

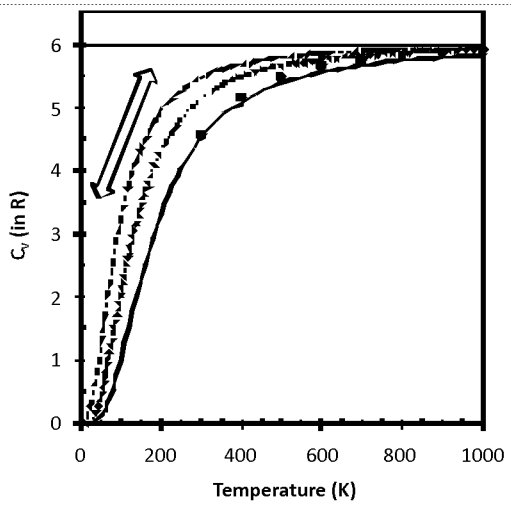

Fig: 4. Constant volume specific heat. Lines have the same meaning as the Fig: 2. Horizontal line indicates high-T Dulong-Petit limit. Experimental data for MgO are taken from [26]

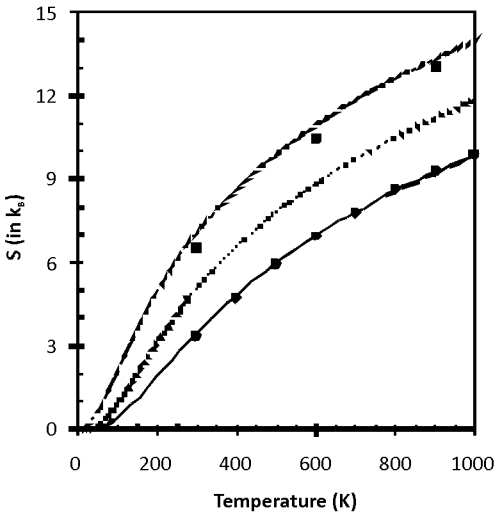

Fig: 5. Entropy as a function of temperature. Lines have the same meaning as the Fig: 2. Experimental data for MgO [26] and SrO [27]

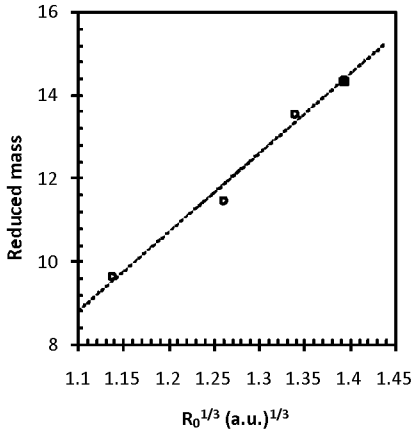

Fig: 6. Variation of reduced mass as a function ionic radius for A^{+2} ion. Filled square indicates the result for BaO in B1-phase

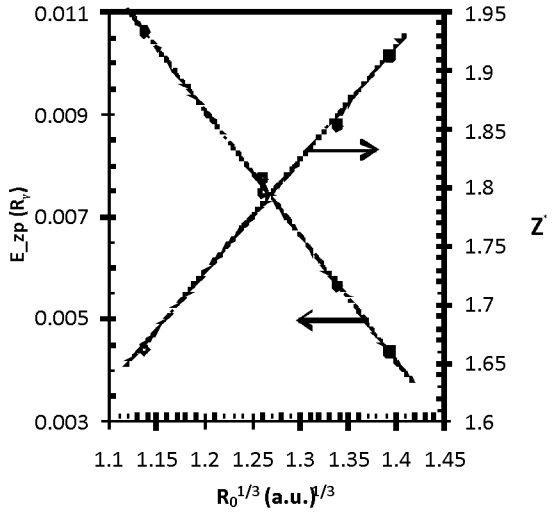

Fig: 7. Zero-point vibrational energy, E_zp, and dynamical effective charge, Z^*, (open circles) are plotted as a function of ionic radius for A^{+2} ion. Filled squares indicate predicted values for BaO. Short-dashed lines represent linear fit to the calculated results.

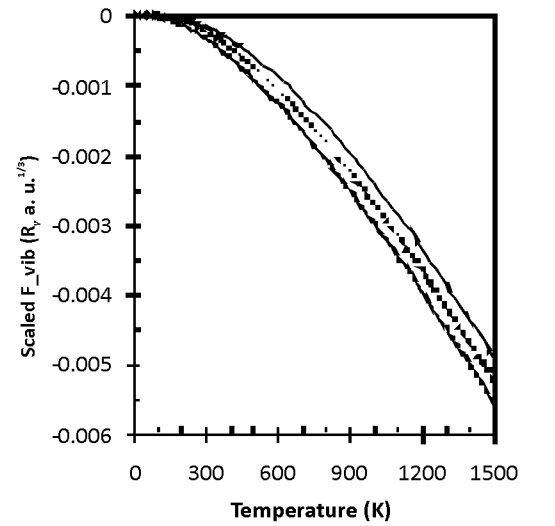

Fig: 8. Scaled vibrational free energy. (See text for more details) Lines have the same meaning as the Fig: 2.

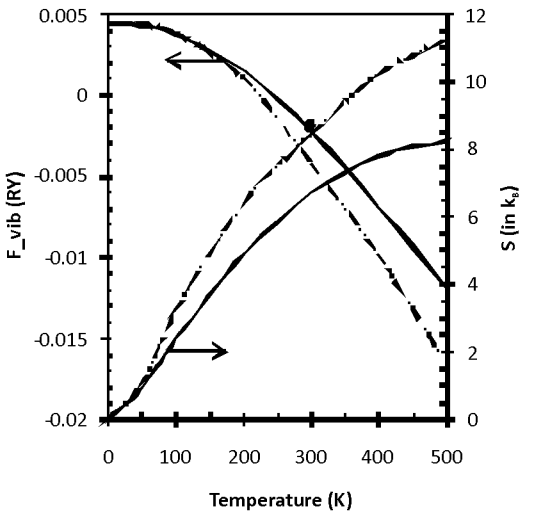

Fig: 9. Predicted phonon vibrational energy and entropy (continuous lines) for B1- phase of BaO. First principle results (dashed-dot lines) due to Lukačević [30] and experimental datum (filled symbol) for entropy is from Ref. [31].

Table: 1. Ground state properties of Alkaline-earth oxides

		a_0 (Å)	B_0 (GPa)	B_0'
MgO	Present	4.237	161.4	4.62
	Expt.	4.213[a]	160.3[a]	4.15[a]
	Others	4.254[c] 4.259[d]	148.6[c] 145.7[d]	4.30[c] 4.23[d]
CaO	Present	4.814	109.0	4.46
	Expt.	4.811[g]	110[g]	4.26[g]
	Others	4.810[i], 4.72[j], 4.820[k]	111.99[i], 128[j], 102[k]	4.39[i], 4.11[j], 4.33[k]
SrO	Present	5.205	89.3	3.84
	Expt.	5.16[m]	91[m]	4.30[m]
	Others	5.073[b], 5.08[c]	92.61[o] 105[n]	5.0[n]

[a]Ref.[9], [b]Ref.[10], [c]Ref.[11], [d]Ref.[12], [e]Ref.[13], [f]Ref.[14], [g]Ref.[15], [h]Ref.[16], [i]Ref.[17], [j]Ref.[18], [k]Ref.[19], [m]Ref.[20], [n]Ref.[21], [o]oRef.[22]

inverse Fourier transform. The phonon dispersion curves were then obtained by interpolating the dynamical matrices using these force constants.

From the calculated phonon density of states g(ω), the thermodynamic properties, e.g., vibrational Helmholtz free energy F_vib, internal energy E_int, constant volume specific heat C_V, and entropy S as a function of temperature are evaluated using the following equations.

$$F\_vib(T) = 6Nk_BT\int \ln\left\{2\sinh\left(\frac{\hbar\omega}{k_BT}\right)\right\}g(\omega)d\omega \quad ...(1)$$

Here, k_B is the Boltzmann constant, N is the normalization constant, ω the phonon frequency, and g(ω)dω represents the p-dos in the frequency interval dω at ω. The constant N is determined such that $\int g(\omega)d\omega = 1$.

Other thermodynamic properties can also be obtained in a similar fashion.

$$E\_int(T) = 3N\hbar\int \omega\left\{\coth\left(\frac{\hbar\omega}{k_BT}\right)\right\}g(\omega)d\omega \quad ...(2)$$

$$S(T) = 6Nk_B\int\left[\left(\frac{\hbar\omega}{2k_BT}\right)\coth\left(\frac{\hbar\omega}{2k_BT}\right) - \ln\left\{2\sinh\left(\frac{\hbar\omega}{2k_BT}\right)\right\}\right]g(\omega)d\omega \quad ...(3)$$

$$C_V(T) = 6Nk_B\int\left(\frac{\hbar\omega}{2k_BT}\right)^2\left[\operatorname{cosec}h\left(\frac{\hbar\omega}{2k_BT}\right)\right]^2 g(\omega)d\omega \quad ...(4)$$

Results and Discussions

Presently computed results for ground state properties are presented in Table 1 for mutual comparison. We see good agreement with experimental and other theoretical results [9-22]. This gives evidence of accuracy of the GGA and the pseudopotential used in the present calculations. With equilibrium volume (V_0) in hand, we proceed to calculate pdc and p-dos for MgO, CaO and SrO in B1-phase. These results are compared with neutron scattering data [20,23-25], and agreement is excellent for all three oxides (Figure-1). In particular, the longitudinal optical (LO) and transverse optical (TO) splitting of the pdc compare nicely with the experimental findings. This advocates the proper inclusion of many-body effect and predicts correct field strength necessary to stabilize anion in such ionic crystals. The positive frequencies of all phonon modes indicate the dynamical stability of AOs in B1-phase. Further, we have calculated partial density of states (though these results are not shown in Fig: 1), the light oxygen atom largely contributes to the high frequency optical vibrations, while the alkaline-earth-metal atoms dominate the acoustic branch of the pdc. Accurate angular phonon vibrational frequencies allow, for B1-phase, the simple calculation of the effective charge Z^* from the relation $(\omega_{LO}^2 - \omega_{TO}^2) = \frac{4\pi(Z^*e)^2}{\mu V_0}$, with μ as reduced mass and e is the electronic charge. These results are presented in Fig: 7 for latter discussion. Based on the p-dos, it is now straight forward to compute basic thermodynamic properties using equations (1)–(4). Results for lattice vibrational free energy F_vib (Fig-2), the internal energy E_int (Fig-3), the constant volume specific heat C_V (Fig-4), and the entropy S (Fig-5) show excellent agreement with the available experimental data [26,27]. The zero-point contribution to F_vib is plotted in Fig: 7. In general, with initial positive contribution, F_vib decreases with temperature crosses zero and finally becomes negative above some characteristic temperature of the material (below which is usually referred to as the quantum regime). We see that from MgO → SrO the characteristic temperature is decreasing. That is, the heavier (larger reduced mass) the cation the smaller is the characteristic temperature. Nevertheless, at higher temperatures F_vib deceases monotonically for all AOs. Similarly, above these temperatures for each AOs, the internal energy linearly increases with temperature (with a slope k_B), indicating that the mean energy of a harmonic oscillator is independent of frequency of oscillation. Although, in the harmonic approximation, high-T limit of C_V is to approach Dulong-Petit law, it deviates strongly for all AOs at low temperatures. Fig: 4 clearly advocates that going from MgO → SrO the area between the constant Dulong-Petit limit and the C_V curve (region marked with double sided arrow in the figure) decreases. In fact, this area gives the measure of characteristic thermal contribution ($k_B\theta$) to the quantum energy; the smaller the area higher is the characteristic temperature θ, and vice versa. For entropy also, we can infer such systematic change going from MgO → SrO. In order to understand and assess this general trend in these oxides, we need parameters or criteria. It is obvious that with heavier alkaline-earth elements, reduced mass will increase. As shown in Fig: 6, when it is plotted as a function of cube root of ionic (A^{+2}) radius (R_0) of the cations, it increases linearly with $R_0^{\frac{1}{3}}$. The linear-fit to these data gives 98.4% correlation. When the value of μ for BaO is inserted in the linear-fit to these data, it predicts 2.7014 a.u. ionic radius for Ba^{+2}. The experimental [28] datum of the same is 2.703 a.u. This observation gives confidence in selecting μ and $R_0^{\frac{1}{3}}$ as parameters to judge the systematic behaviour of these oxides. Further, Ohta et al. [29] have studied divalent ions substituted single crystals $0.95(Na_{0.5}Bi_{0.5})TiO_3$–$0.05(M)TiO_3$ perovskite, where M represents Ca, Sr or Ba. They employed inelastic light scattering technique for measuring the dielectric constant, and the Raman and the Brillouin scattering in order to investigate the difference in the substitution effect among Ca^{+2}, Sr^{+2}, and Ba^{+2} ions on the electric property, the acoustic phonon and the optical phonon. They found the dielectric constant along the c-axis increase with increasing radius of substituted ions. Motivated by this observation in the present study, we have plotted, a rather closely related physical property the effective valence (Z^*) of cations versus $R_0^{\frac{1}{3}}$ in Fig: 7. We find Z^* scales linearly with $R_0^{\frac{1}{3}}$ also. Finally, in order to have proper low-T dependence of vibrational free energy, we have plotted the $R_0^{\frac{1}{3}}$ dependence of zero-point vibration energy, see Fig: 7. Linear dependence of Z^* and E_zp is used to estimate Z^* and E_zp of BaO. For instance, the present zero-point energy 4.351 mRy compares within the 3.3% with recent *ab initio* findings [30], 4.494 mRy. Based on the linear scaling of μ, Z^* and E_zp with respect to $R_0^{\frac{1}{3}}$ we have scaled vibrational free energy F_vib by multiplying with a factor

$\frac{R_0^3}{\mu Z^{*2}}$ These results for scaled F_vib at different temperature minus the scaled F_vib at T = 0 K for three AOs are presented in Fig: 8. One can notice that all three graphs very similar to each other with maximum deviation from lowest to highest values is about 16.7% at T =1000 K. This universal behaviour of lattice vibrational free energy can be fitted to the cubic polynomial of the type $F(T) = aT^3 + bT^2 + cT$; with fitting parameters a=1.9591.10^{-12}, b=–4.5618.10^{-9}, c=3.6045.10^{-7} with appropriate units. Including the deviation in graphs of scaled F_vib, our careful analysis these fitting parameters suggests that the F(T) can be reliable within the 24%. Using this scaling law, the phonon thermal free energy and then determined entropy are compared in Fig: 9 with recent full lattice dynamics based findings [30]. Only qualitative agreement is observed with other calculated thermal properties. The discrepancy observed in computed results can be attributed to the poor estimation of Z^* through much simpler method. Present result for effective charge is too small compared to 1.96, 2.39, and 2.49 for MgO → SrO, respectively, reported by Bousquet et al. [5]. These authors have attributed high Z^* to oxygen 2p-metal d hybridizations to atomic displacements. In order to calculate this effect accurately, one requires knowing the response of ions to the external electric field of surrounding ions. However, no such attempt was made in the present study, and only simpler formula was used to estimate Z^*. Thus, inaccuracy in the scaling factor Z^* is reflected in other properties.

Summary and Conclusion

We have employed first principles pseudopotentials DFPT technique to compute phonon dynamics of cubic MgO, CaO and SrO. Their high-T thermodynamics is deduced within the harmonic approximation. We have then proposed a simple linear scaling criterion to estimate thermal properties of these oxides. A simple scheme which relies on scaling factor made up of ionic radius, reduced mass, effective charge and zero-point energy is applied to BaO. The scaling law is based on the observation that, e.g., polarizability of these oxides and therefore other optical and electric properties increase going from BeO → BaO indicating a systematic change in observed properties. However, due to different crystal structure (B8-phase), the same linear scaling may be a suspect, and we have excluded BeO from our scheme. Results for vibrational energy and entropy for BaO shows general trend in agreement with recent lattice dynamical based findings [30]. Discrepancies in these results can be attributed to poor estimation of Z^*, and may be uncertainty in determining R_0 for cations. In the present study, the chosen R_0 was for divalent cations, while the effective charge is different. Thus one may expects change in R_0 too. Nevertheless, considering the mathematical ease, we believe that the present scaling scheme is satisfactory. We further conclude that based on similar argument and through systematic comparison among same group compounds one can estimate different physical properties as well.

Acknowledgement

The author is grateful to Dr. A. Y. Vohra for help in running the Quantum Espresso code, and the UGC, New Delhi for financial assistance under the Major Research Project No. 42-771/2013(SR).

REFERENCES

[1] Anderson, O.L. (1995) *Equation of state for geophysics and ceramics science*, Oxford University Press, New York.

[2] Neudeck, P.G., Okojie, R. S. and Chen, L. –Y. (2002) High-temperature electronics–A role for wide bandgap semiconductors? *Proceedings of the IEEE*, Vol. 90, pp. 1065-1076.

[3] Hubbard, K.J. And Schlom, D.G. (1996) Thermodynamic stability of binary oxides in contact with silicon. *J. Mater. Res.*, **11**: 2757-2776.

[4] Dafang, L., Zhang, F. and Yan, J. (2014) Ab initio molecular dynamics study of high-pressure melting of beryllium oxide. *Sci. Rep.*, **4**: 4707(05).

[5] Bousquet, E., Spaldin, N.A. and Ghosez, P. (2010) Strin-induced ferroelectricity in simple rocksalt binary oxides. *Phys. Rev. Lett.*, **104**: 037601(04).

[6] Baroni, S., de Gironcoli, S., Corso, A. and Gianozzi, P. (2001) Phonons and related crystal properties from density-functional perturbation theory. *Rev. Mod. Phys.*, **73**: 515-562. www.pwscf.org

[7] Perdew, J. P. and Wang, Y. (1992) Accurate and simple analytic representation of the electron-gas correlation energy. *Phys. Rev. B*, **45**: 13244-13249.

[8] Murnaghan, F.D. (1944) The compressibility of media under extreme pressures. *Proc. Natl. Acad. Sci.*, **30**: 244-247.

[9] Fei, Y. (1999) Effects of temperature and composition on the bulk modulus of (Mg. Fe)O. *Am. Miner.*, **84**: 272-276.

[10] Chang, K.J. and Cohen, L.M. (1984) High-pressure behavior of MgO: Structural and electronic properties. *Phys. Rev. B*, **30**: 4774-4786.

[11] Schleife, A., Fuchs, F., Furthmuller, J. and Bechstedt, F. (2006) First-principles study of ground- and excited-state properties of MgO, ZnO, and CdO polymorphs. *Phys. Rev. B*, **73**: 245212(1-14).

[12] Gueddim, A., Bouarissa, N. and Villesuzanne, A. (2009) First-principles determination of structural properties of MgO. *Phys. Scripta*, **80**: 055702(1-3).

[13] Baranov, A.N., Stepanyuk, V.S., Hergert, W., Katsnelson, A.A., Settels, A., Zeller, R. and Dederichs, P.H. (2002) Full-potential KKR calculations for MgO and divalent impurities in MgO. *Phys. Rev. B*, **66**: 155117(1-4).

[14] Causa, M., Dovesi, R., Pisani, C. and Roetti, C. (1986) Electronic structure and stability of different crystal phases of magnesium oxide. *Phys. Rev. B*, **33**: 1308-1316.

[15] Richet, P., Mao, H.K. and Bell, P.M. (1988) Static compression and equation of state of CaO to 1.35 Mbar. *J. Geophys. Res. Lett.*, **93**: 15279-15288.

[16] Cortonay, P. and Monteleone, A.V. (1996) Ab initio calculations of cohesive and structural properties of the alkali-earth oxides. *J. Phys.: Condens. Matter*, **8**: 8983–8994.

[17] Deng, Y., Jia, O.H., Chen, X.R. and Zhu, J. (2007) Phase transition and elastic constants of CaO from first-principle calculations. *Physica B*, **392**: 229-232.

[18] Baltachea, H., Khenataa, R., Sahnounb, M., Driza, M., Abbarc, B. and Bouhafsc, B. (2004) Full potential calculation of structural, electronic and elastic properties of alkaline earth oxides MgO, CaO and SrO. *Physica B*, **344**: 334-342.

[19] Mehl, M.J., Hemley, R.J. and Boyer, L.L. (1986) Potential-induced breathing model for the elastic moduli and high-pressure behavior of the cubic alkaline-earth oxides. *Phys. Rev. B*, **33**: 8685-8696.

[20] Galtier, M., Montaner, A. and Vidal, G. (1972) Optical Phonons of CaO, SrO, BaO at the Center of the Brillouin Zone at 300 and 17 K. *J. Phys. Chem. Solids*, **33**: 2295-2302.

[21] Karki, B.B., Wentzcovitch R.M., de Gironcoli S. and Baroni S. (1999) First-Principles Determination of Elastic Anisotropy and Wave Velocities of MgO at Lower Mantle Conditions. *Science*, **286**: 1705-1707.

[22] Souadkia, M., Bennecer, B. and Kalarasse, F. (2012) Ab initio lattice dynamics and thermodynamic properties of SrO under pressure. *J. Phys. Chem. Solids*, **73**: 129-135.

[23] Sangster, M.J.L., Peckham, G., Saunderson, D.H. (1970) Lattice dynamics of magnesium oxides. *J. Phys. C*, **3**: 1026-1036.

[24] Saunderson, D.H. and Peckham G. (1971) The lattice dynamics of calcium oxide. *J. Phys. C*, **4**: 2009-2016.

[25] Rieder, K.H., Migoni, R. and Renker B. (1975) Lattice dynamics of strontium oxide. *Phys. Rev. B*, **12**: 3374-3379.

[26] Anderson, O.L. and Zou, K. (1990) Thermodynamic functions and properties of MgO at high compression and high temperature. *J. Phys. Chem. Ref. Data*, **19**: 69-81.

[27] Cordfunke, E.H.P., van der Laam, R.R. and van Miltenburg, J.C. (1994) Thermophysical and thermochemical properties of BaO and SrO. *J. Phys. Chem. Solids*, **55**: 77-84.

[28] www.docbrown.info/page07/sblockb.htm, www.springerreference.com/docs/html/chapterdbid/30181.html.

[29] Ohta, R., Onda, Y. and Kojima, S. (2011) Inelastic light scattering of divalent ions (Ca^{2+}, Sr^{2+}, and Ba^{2+}) substituted ($Na_{1/2}$, $Bi_{1/2}$)TiO_3 single crystals. *J. Korean Phys. Soc.*, **59**: 2471-2474.

[30] Lukačević, I. (2011) High-pressure lattice dynamics and thermodynamics in BaO. *Phys. Status Solidi B*, **248**: 1405-1411.

[31] Linstrom, P.J. and Mallard, W.G. (Eds.) (2008) NIST Standard Reference Database Number 69 (National Institute of Standards and Technology, Gaithersburg MD). http://webbook.nist.gov.